Boundary-Layer Meteorol (2007) 123:269–294
DOI 10.1007/s10546-006-9140-y

ORIGINAL PAPER

Negative water vapour skewness and dry tongues in the convective boundary layer: observations and large-eddy simulation budget analysis

F. Couvreux · F. Guichard · V. Masson · J.-L. Redelsperger

Received: 18 April 2006 / Accepted: 30 October 2006 / Published online: 23 December 2006

Abstract This study focuses on the intrusion of dry air into the convective boundary layer (CBL) originating from the top of the CBL. Aircraft in-situ measurements from the IHOP_2002 field campaign indicate a prevalence of negative skewness of the water vapour distribution within the growing daytime CBL over land. This negative skewness is interpreted according to large-eddy simulations (LES) as the result of descending dry downdrafts originating from above the mixed layer. LES are used to determine the statistical properties of these intrusions: their size and thermodynamical characteristics. A conditional sampling analysis demonstrates their significance in the retrieval of moisture variances and fluxes. The rapid CBL growth explains why greater negative skewness is observed during the growing phase: the large amounts of dry air that are quickly incorporated into the CBL prevent a full homogenisation by turbulent mixing. The boundary-layer warming in this phase also plays a role in the acquisition of negative buoyancy for these dry tongues, and thus possibly explains their kinematics in the lower CBL. Budget analysis helps to identify the processes responsible for the negative skewness. This budget study underlines the main role of turbulent transport, which distributes the skewness produced at the top or the bottom of the CBL into the interior of the CBL. The dry tongues contribute significantly to this turbulent transport.

Keywords Convective boundary layer · Dry tongues · Large-eddy simulation · Skewness · Variance · Water vapour

1 Introduction

The water vapour field exhibits strong variability across a wide range of scales from planetary, synoptic down to small-scale turbulence. This variability plays an impor-

F. Couvreux (✉) · F. Guichard · V. Masson · J.-L. Redelsperger
GAME-Météo-France CNRM/GMME
42 avenue G. Coriolis, 31057 Toulouse Cedex 1, France
e-mail: fleur.convreux@meteo.fr

tant role in several major areas of the atmospheric science such as cloud formation, radiation and climate. The variability at low levels has an impact on the initiation of cloud, the development of convective storms, and more broadly on the hydrological cycle. A few observational studies have provided some information concerning the water vapour distribution in the boundary layer. Yet, this variability is not fully understood. In the convective boundary layer (CBL), organized structures such as rolls and cells tend to homogenise the water vapour vertical structures via turbulent vertical mixing, whereas they generate moisture heterogeneities in the horizontal, with thermals typically moister than their surroundings. Entrainment, corresponding to a negative heat flux at the top of the CBL, is important for the water vapour variability as has been underlined by Coulman (1978) and Tuzet et al. (1983). The growth of the CBL and the humidity step at the top of the CBL also play a role in determining the humidity variance (Druilhet et al. 1983). The former study analysing the potential temperature-moisture correlation of aircraft measurements taken around noon identifies 'entrained cells' up to the middle of the boundary layer.

Distributions of water vapour mixing ratio (r_v) in the CBL derived from aircraft in-situ data indicate the complex structure of this field (Crum and Stull 1987; Weckwerth et al. 1996), which is not properly represented by a simple Gaussian distribution. Weckwerth et al. (1996) reported a range of fluctuations on the order of 1.5 to 2.5 g kg^{-1} (for a mean value around 15 g kg^{-1}) for r_v in the mixed layer, and related these fluctuations to the occurrence of convective rolls. Crum and Stull (1987) and Weckwerth et al. (1996) noted a negative skewness of r_v within the CBL. Such a negative skewness of r_v in the upper part of the boundary layer is also reported by other observational studies (Young et al. 2000; Vila-Guerau de Arellano et al. 2004). Mahrt (1991) derived skewness from low-altitude aircraft (150 m above ground level) moisture measurements, and on occasions found negative skewness in the lower part of the boundary layer that he interpreted as the evidence of deep penetration of drier air from the CBL top. In fact, a negative skewness reflects the occurrence of strongly negative anomalies. For a cloud-free CBL, in the absence of strong advection, a common source of dry air for the mixed layer is the free troposphere above. Therefore, a negative skewness of r_v within the CBL can be related to the existence of intrusions of dry air from above. Mahrt (1991) proposed to distinguish between two types of boundary-layer moisture regimes according to the r_v skewness in the lower part of the boundary layer: an entrainment drying boundary layer (EDBL), with negative skewness, and a moistening boundary layer (MBL) with positive skewness. Note that these prototypes are based on low-level measurements. Using a simplified budget analysis, he linked this negative skewness to the divergence of moisture flux at these levels. Such a relationship between skewness and the flux profile, if observed, would help to infer vertical flux profiles that are typically very difficult to measure. In fact, reliable flux profile determination requires long aircraft flight legs (in order to reduce the sampling error, see Lenschow et al. 2000) at different levels, which are difficult to obtain simultaneously. Besides the observations of Mahrt (1991) focusing on the lower CBL, there is no consensus among the few existing studies on the relationship between moisture skewness and moisture flux vertical profiles in the CBL (Wulfmeyer 1999).

In the present study, we use high-resolution simulations as a complement to observations to characterise the dry tongues arising from the top of the CBL that are responsible for negative moisture skewness. The observations were obtained during the International H_2O Project (IHOP_2002) a field experiment dedicated to the

measurement of water vapour (Weckwerth et al. 2004). Recently, Couvreux et al. (2005, C05 in the following) found that high-resolution simulations were able to reproduce the observed CBL water vapour variability during IHOP_2002 at horizontal scales smaller than 10 km; dry downdrafts originating from the top of the boundary layer were identified. The present study complements these results, and the main objective is to further characterise these dry downdrafts. Firstly, we quantify their contribution to the moisture distribution, variance and flux in the CBL. Secondly, we analyse the buoyancy of the dry tongues and its evolution as the tongues reach lower levels. We propose an explanation for their kinematics within a rapidly growing CBL. Thirdly, we investigate the robustness of the relationship proposed by Mahrt (1991) between the moisture flux divergence and the sign of the moisture skewness in the lower CBL. We wish to assess how this relationship extends to the whole boundary layer and relate it to relevant physical processes. This is achieved with high-resolution simulations that enable us to retrieve a comprehensive budget of skewness over the whole depth of the boundary layer.

The outline of the paper is as follows. Section 2 presents the data and the two simulations used in the study. A detailed presentation of the water vapour moments in both simulations is also given. Section 3 documents the main characteristics of these intrusions according to IHOP_2002 observations and high-resolution simulations and assesses the role of such intrusions in the boundary-layer statistical properties. Section 4 is dedicated to process analyses, and focuses firstly on the buoyancy field, an important actor in the explanation of some properties of the intrusions. Secondly, budgets of variance and third-order moment of water vapour mixing ratio are presented. The main processes responsible for the asymmetry are then identified using the moisture skewness budget. Finally, conclusions are drawn in Section 5.

2 Data and simulations

In this study, we combine IHOP_2002 observations (in-situ aircraft measurements and radiosondes mainly) with large-eddy simulations (LES).

2.1 Observations

During IHOP_2002, intensive observing periods (IOP) focusing on the boundary layer were divided into two groups (Weckwerth et al. 2004): the boundary-layer evolution IOPs (BLE) were dedicated to the analysis of the growing phase of the boundary layer from early morning to early afternoon, and the boundary-layer heterogeneity IOPs (BLH) focused on the developed CBL in the afternoon. Observations (soundings and aircraft measurements) from both BLE and BLH IOP are used in this study. A total of 35 h of the University of Wyoming King Air aircraft data divided into 148 legs (at different levels, see Table 1) were used to investigate moisture variability. These flights corresponded to successive legs at different altitudes from 60 m above the surface to the upper boundary layer alternatively for the BLH, whereas for the BLE flights the aircraft flew at one or two constant altitudes in the lower half of the CBL. Boundary-layer heights (z_i) derived from airborne lidar observations (Davis et al. 2000) were used for each aircraft leg.

Eleven days (8 BLH and 3 BLE) were investigated; a brief summary of their main characteristics is given in Table 1. There is a wide variety of conditions (different wind

Table 1 Characteristics of the different IOP days used in this study: date, type of IOP, hours of the IOP, length of the UWKA aircraft legs, area considered (Hom for the western area of the IHOP domain, Cent for the central area and East for the eastern area; see Weckwerth et al. 2004 for more details), duration after last rain event (assessed from surface stations measurement), wind speed (maximum) and direction, latent heat flux (maximum), water vapour mixing ratio, potential temperature (maximum) measured at the surface by the ISFF stations located in the area considered during the flight hours, moisture and potential temperature differences at the top of the boundary layer inferred from soundings (for mission over the western area, the ISS sounding at 1200 was used) and maximum of boundary-layer height (hBL) derived from lidar data

days	BLE/ BLH	Timing (local h)	legs (km)	area	days /rain	wind ms^{-1}/dir	r_v ($g\,kg^{-1}$)	θ (K)	LvE ($W\,m^{-2}$)	Δr_v ($g\,kg^{-1}$)	$\Delta\theta$ (K)	hBL (m)
19 05	BLH	1200–1400	45	Hom	2	12 /160	7	302	100	~0	5	1370
20 05	BLH	1200-1430	45	Hom	3	11 /140	6	303	70	1,5	5	1200
21 05	BLH	1330-1600	50	Cent	2	10 /140	10	297	70-330	3	5	1720
25 05	BLH	1200-1430	50	Hom	1	5 /0	8	298	200	3	4	1250
29 05	BLH	1200-1430	50	Hom	1	7 /190	12	308	340	5	4	1400
07 06	BLH	1200-1430	45	Hom	2	10 /170	10	310	100-240	3	2	1500
14 06	BLE	1000-1230	70	Hom	1	5 /30	12	305	200-250	4,5	4	1050
16 06	BLH	1200-1500	55	Cent	1	3 /0	12	299	200-330	3	3	1450
17 06	BLH	1200-1400	45	East	2	7 /200	13	301	100-350	6	5	1200
21 06	BLE	1100-1330	65	Hom	3	11 /170	13	306	120-160	2	1	1250
25 06	BLE	1100-1400	35	Hom	7	7 /150	10	310	60-130	3	3	1470

The flights over the western area were oriented north-south for the BLH cases and west-south-west/east-north-east for the BLE cases. The flights over central and eastern areas were oriented west/east. Note that there are uncertainties in the estimate of moisture surface fluxes (spread between the different surface flux stations) and moisture and temperature gradient at the top of the boundary layer inferred from soundings (representativeness of the soundings)

speed, wind direction, duration since the last rain event, surface heat fluxes, water vapour mixing ratio and temperature). Note that, for the 21 June 2002 boundary-layer heights were deduced from soundings as no airborne lidar data were available. Some rough subsidence estimates were derived from soundings, and ranged from 5 to 20 $mm\,s^{-1}$. Moisture soil availability was larger to the east than to the west.

Since we focus on processes at the sub-mesoscale (scale <10 km), the aircraft measurements were filtered with a 10-km running mean so as to remove the variability due to scales greater than 10 km. The aircraft data were available at 1 Hz corresponding to a spatial resolution of approximately 90 m (the aircraft velocity was around 90 $m\,s^{-1}$). The mixing ratio was derived from the thermo-electric hygrometer.

2.2 LES simulations

Two different simulations are used: the first, hereafter referred to as REF, is similar to the reference simulation described in C05 except with higher resolution. The second, hereafter referred to as CSTINI, is a sensitivity case beginning with a constant and dry profile, similar to the CBL observed on the 19 May as discussed later. These simulations have been performed with the LES version of the non-hydrostatic model Meso-NH (Lafore et al. 1998); the subgrid model is a turbulence model based on a prognostic equation for the turbulent kinetic energy with a Deardorff mixing length scale (Cuxart et al. 2000).

The set-up of the REF experiment is based on observations and designed to represent a mostly clear day with light winds (less than 5 $m\,s^{-1}$). It focuses on the diurnal

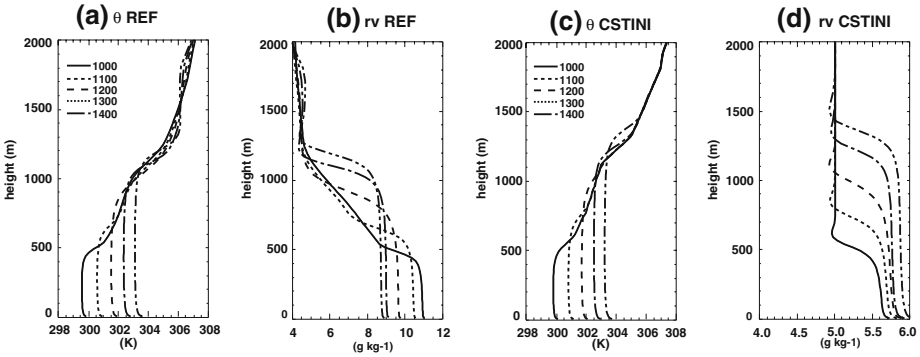

Fig. 1 Vertical profile (as a function of height) of the mean potential temperature and water vapour mixing ratio from the REF (**a** and **b**) and CSTINI simulations (**c** and **d**). Note that different scales are used for the water vapour mixing ratio axis in order to resolve the differences

development of the boundary layer from early morning to early afternoon with an integration time of seven hours (C05). Initial profiles obtained from a composite of soundings and time-varying surface fluxes derived from observations were prescribed. Large-scale (greater than 10 km) advection of temperature and moisture and subsidence were also accounted for.[1] This LES has been extensively validated with IHOP_2002 observations (soundings, aircraft and lidar measurements: C05), and this former study focused on the ability of LES to represent the water vapour variability. Here, the simulation is used to understand processes controlling moisture variability. To better represent processes at the top of the boundary layer and narrow dry tongues within the CBL, the simulation has been re-run with higher resolution: a horizontal resolution of 50 m and a vertical stretched grid containing 75 levels with vertical resolution finer than 25 m below 2000 m (the CBL top maximum is around 1500 m) and coarser resolution higher up. The domain size is $10 \times 10 \times 4\,\mathrm{km}^3$. Besides the modification of resolution and domain, the same configuration as in C05 is used. The profiles of the mean potential temperature and water vapour mixing ratio are shown in Fig. 1a and b. The growth of the CBL is apparent, and started at 500 m at 1000 local time (LT, where LT = UTC − 5) up to 1200 m at 1400 LT. The CBL warms during the day in response to increased surface heat fluxes. The drying of the boundary layer is indicated by a stronger moisture flux at the CBL top than at the surface (Fig. 2b). The moisture variance (Fig. 2c) has its maximum at the boundary-layer top and this maximum increases during the day up to 1200 LT, when the humidity step at the CBL top is the largest (Fig. 2a). The r_v skewness is negative within most of the CBL (Fig. 2e) and over time, the only significant variation with time is a slight decrease of the skewness as the CBL grows. Above the CBL top the r_v skewness is positive. In the following, the moisture skewness will refer to the r_v skewness, denoted by S and defined by:

$$S = \frac{\overline{r_\mathrm{v}'^3}}{[\overline{r_\mathrm{v}'^2}]^{3/2}},$$

[1] Initial profiles, prescribed surface fluxes, large-scale advection and wind profiles are reported in the Appendix of C05.

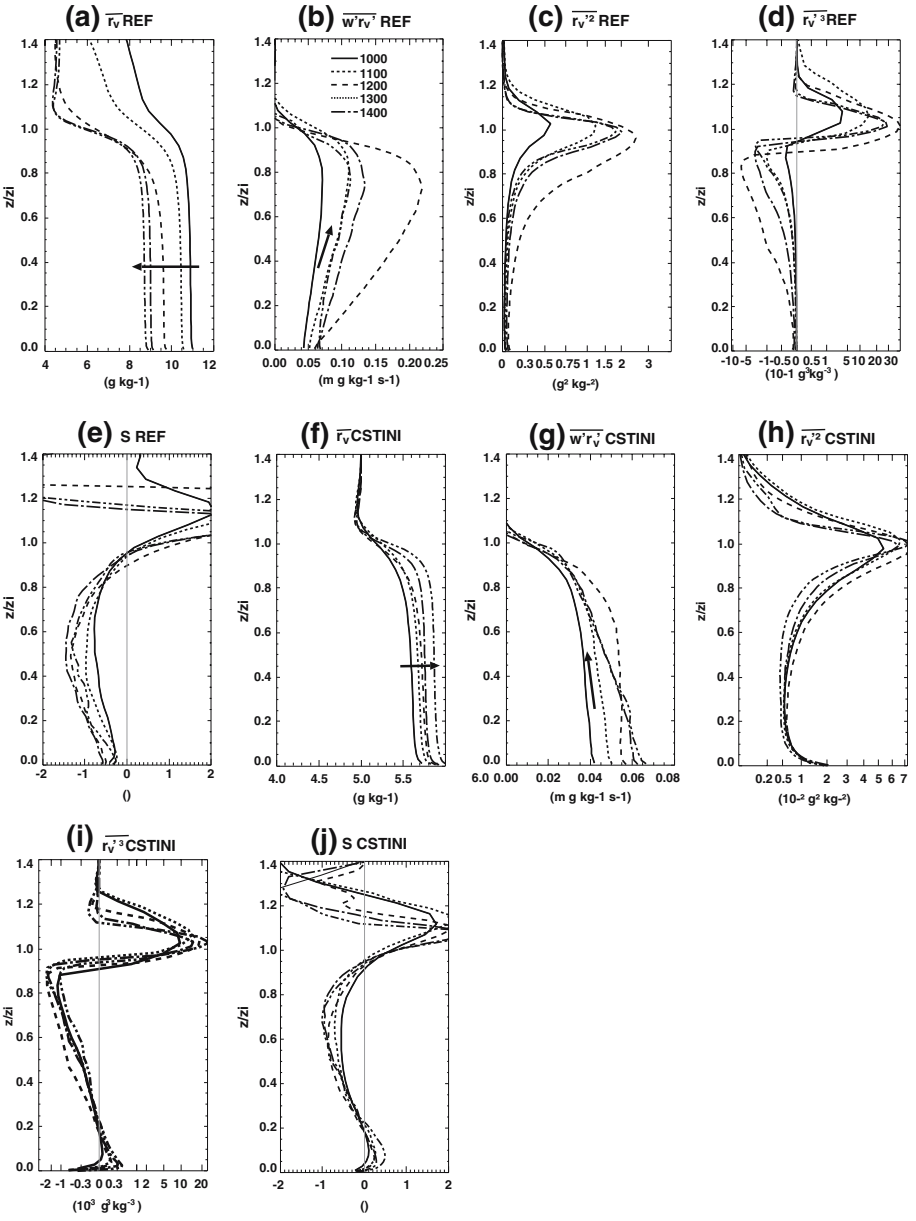

Fig. 2 Vertical profile (as a function of z/z_i) of water vapour mixing ratio mean, flux, variance, third-order moment and skewness from the REF (panels **a**, **b**, **c**, **d**, **e**) and CSTINI simulations (panels **f**, **g**, **h**, **i**, **j**). Different scales are used for the simulations in order to resolve the differences and non-linear scales are used for the x-axis for the variance and third-order moment in order to show the values in the mixed layer and the entrainment zone

where the overbar indicates the average over the domain of the simulation (or over the flight leg for observations) and the prime the deviation from the domain mean value (the 10-km running mean for observations).

CSTINI uses the same set-up as REF except that the initial r_v profile is constant and equal to a value of $5\,g\,kg^{-1}$ (Fig. 1d). Time-varying surface latent and sensible heat fluxes are prescribed, exactly as in REF, with the same values. Note also that large-scale advection and subsidence have not been accounted for in this simulation.[2] This lack of subsidence explains in part the deeper CBL. Fig. 2f–j show the profiles of the different moments of r_v. The boundary layer moistens during the simulation due to the surface evaporation being stronger than the moisture flux at the CBL top (Fig. 2g). The mean water vapour mixing ratio increases even though it is highly diluted by the growth of the boundary layer. The variance, $\overline{r_v'^2}$, is much less than in REF (more than 10 times smaller) but the vertical profile is similar with a maximum at the CBL top (Fig. 2h). The skewness profile is more complicated as there are positive values at low levels up to $0.2z_i$ and negative values higher into the CBL (Fig. 2j). The magnitude of S is similar to that in REF even though the variance (Fig. 2h and c) and the third-order moment (Fig. 2i and d) are much smaller, underlining the compensation between both moments in the S computation. This simulation has similarities with the 19 May 2002 IHOP_2002 case, since the r_v profile is almost constant and the fluxes at the top of the boundary layer are weak due to a small moisture gradient at this level.

Note here that these simulations differ in their r_v mean profile and their moisture flux profile: REF is characterised by a divergence in the moisture flux in the boundary layer, inducing a drying of the CBL, whereas CSTINI is characterised by a convergence of the moisture flux leading to a moistening of the boundary layer. Thus, it is not possible to simply link the skewness sign with the mean boundary-layer vertical divergence as the skewness changes its sign along the CBL in CSTINI. The CSTINI simulation was performed in order to obtain a simulation characterised by a convergence of the moisture flux, with the moisture flux at the surface exceeding the moisture flux at the top of the boundary layer. In such a simulation, the upward moisture transport should be prevalent. The objective pursued here is to determine whether the relationship between the sign of the moisture flux divergence and the sign of moisture skewness (opposite signs) in the lower CBL as proposed by Mahrt (1991) can be extended to the whole boundary layer. According to both simulations, this relationship is complex, as the skewness can vary with height in the CBL. Figure 3 shows that this relationship (opposite signs of S and flux divergence) is valid at low levels where it was proposed by Mahrt (1991): for the layer $[0.1z_i, 0.2z_i]$, S is negative while the flux divergence is positive in REF, while the opposite occurs in CSTINI. However, it does not hold for the whole boundary-layer depth where vertical fluctuations are important: S becomes negative in CSTINI as well, despite a negative flux divergence. A comprehensive budget of S is presented in Section 4.2.

3 Characterisation of the 'dry tongues'

The negative skewness of the water vapour mixing ratio in the boundary layer reflects the occurrence of highly negative perturbations (Mahrt 1991; Lenschow et al. 2000).

[2] These forcings do not much affect the CBL water vapour variability but were prescribed in REF so as to more closely follow the observed situation.

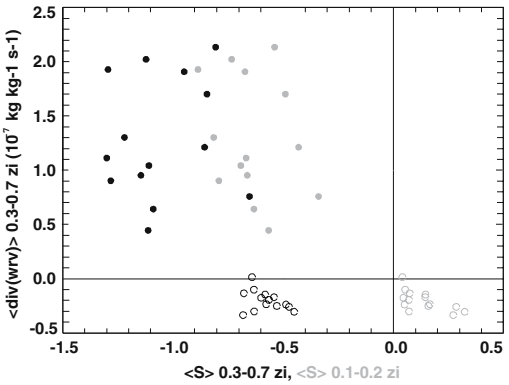

Fig. 3 Flux divergence in the CBL (between $0.3z_i$ and $0.7z_i$) as a function of S from the middle of the CBL (average between $0.3z_i$ and $0.7z_i$) in black and as a function of S from the lower part of the CBL (average between $0.1z_i$ and $0.2z_i$) in grey. The full (empty) circles correspond to the REF (CSTINI) simulation from 1000 to 1400–LT

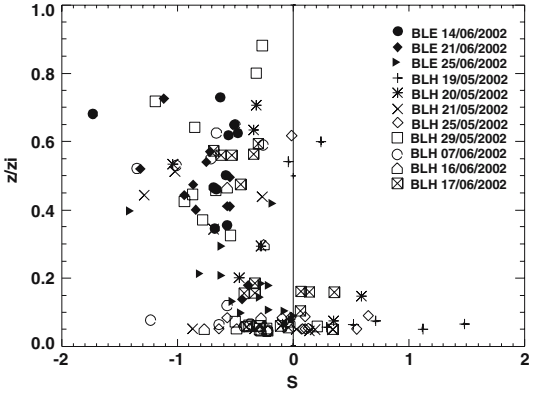

Fig. 4 Vertical profile of skewness derived from aircraft in-situ measurements during 11 days of IHOP_2002. The full symbols correspond to BLE IOP days whereas empty symbols correspond to BLH IOP days (see text for definition of such IOPs). Here, z_i has been determined from lidar aerosol profiles except for 21 June 2002 where z_i has been determined from soundings

These perturbations are referred to as "dry tongues", in accordance with the morphology of these structures. In this section, we use IHOP_2002 observations and LES results to investigate the characteristics of 'dry tongues'.

3.1 Evidence of 'dry tongues' in IHOP_2002 data

As shown in C05, dry tongues are evident in water vapour measurements made with the differential absorption lidar. In order to assess the representativeness of the 14 June 2002 case, aircraft in-situ moisture measurements taken during the eleven days described in Section 2 were analysed. S is calculated using the deviation from a 10-km running mean computed for each leg (see Table 1 for leg lengths).

The mesoscale (horizontal scales larger than 10 km) r_v variability changes from day to day but, nevertheless, for all 11 days fluctuations are noted at scales smaller than 10 km. The time series indicate the frequent occurrence of intrusions of dry air, as is also reflected in the negative S in the CBL on most of the days (Fig. 4).

Only one IOP (19 May 2002) has a constant positive S at nearly all levels in the CBL. This day is characterised by a very particular profile of r_v, as indicated in Fig. 5a. First, r_v is low in the CBL with a mean value around 6.5 g kg^{-1}, which hardly changes during the day as attested by soundings (Fig. 5a) and surface stations. There is a very small jump in moisture just above the CBL (Table 1). The potential temperature capping inversion is strong (>4 K) and the wind speed is significant (around 15 to 20 m s^{-1}).

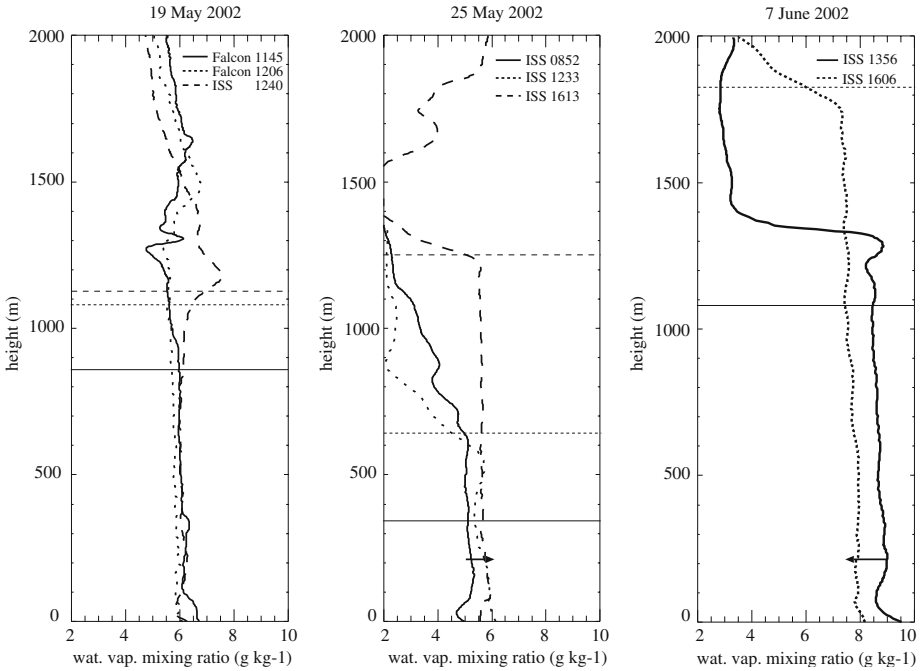

Fig. 5 Vertical profile of water vapour mixing ratio measured by soundings for 19 May 2002 (left panel; Falcon dropsondes and ISS soundings), 25 May 2002 (middle panel; ISS soundings) and 7 June 2002 (right panel; ISS soundings). The horizontal line corresponds to the CBL height derived from the potential temperature profile of the same sounding. Arrows denote the temporal order of the soundings

It seems that the positive skewness on this day is linked to the very small moisture gradient at the top of the boundary layer, and therefore to a very small moisture flux at the CBL top (not shown). Moreover, the surface latent heat flux is small.

Four days have both negative and positive S, with positive S located at low levels. As an example, on 25 May 2002, positive S was recorded during low-level legs. During this day, winds are rather weak (below $5\,\mathrm{m\,s^{-1}}$) and a slight moistening is indicated by soundings (Fig. 5b). No conclusion on the necessary conditions that prevail for the existence of positive S can be drawn due to the small amount of days; nevertheless on all of these days, a moistening of the CBL is observed as the mean r_v in the CBL remains stationary or increases while the CBL grows, indicating positive moisture flux. Moreover, they all have a relatively small moisture gradient at the top of the CBL relatively to the potential temperature gradient, except for the 17 June.

Six days have a negative S. These days occur late in the IHOP_2002 period (end of May or June). Particularly, during the growing phase of the boundary layer (BLE cases), a systematic and significant negative S is noted. But BLH cases such as 7 June also show a negative S. On this day, the boundary layer grows to a depth of 1800 m and its mean water vapour mixing ratio decreases during the day (Fig. 5c). All these days are characterised by a relatively large moisture gradient at the top of the CBL. The wind does not seem to affect the sign of S: for example, on 14 June the wind speed is low ($<5\,\mathrm{m\,s^{-1}}$) and on 21 June the wind speed is moderate to strong ($>10\,\mathrm{m\,s^{-1}}$).

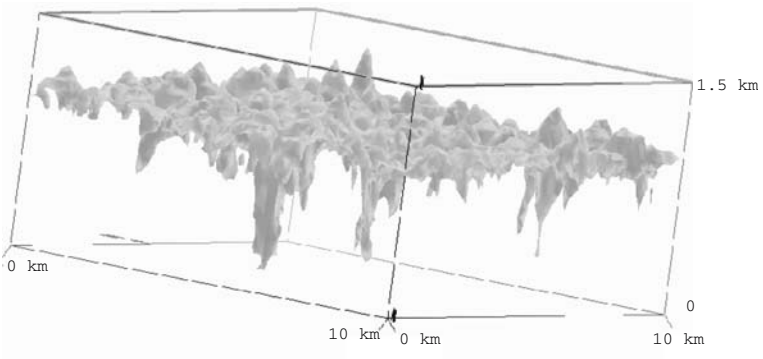

Fig. 6 3D view of the level 7.7 g kg^{-1} of water vapour mixing ratio around 1300 LT for the REF simulation. For clarity, only the lowest 1.5 km of the domain is shown

Note that this negative S is observed even close to the ground, emphasizing the very deep entrainment. In addition, aircraft measurements for the 14 June 2002 indicate a negative S (C05, their Fig 14) and the differential absorption lidar shows the existence of dry tongues (C05, their Fig 13b).

To sum-up the analysis, even though it is difficult to determine the characteristics that cause positive or negative S, we note the prevalence of negative S in the CBL during this springtime period over the Southern Great Plains area. This underlines the importance of entrainment mechanisms down to very low levels, especially when the convective boundary layer is growing rapidly. Moreover, the strength of the moisture gradient at the top of the CBL seems to condition partly at least the sign of S. Negative S in the boundary layer inferred from aircraft measurements was also noted for a Sahelian convective boundary layer under semi-arid conditions by Lothon et al. (2005) and was reported also by Young et al. (2000) and Vila-Guerau de Arellano et al. (2004). In the following, we use large-eddy simulations to study the characteristics that prevail for negative S.

3.2 Evidence of 'dry tongues' in LES

In C05 (their Fig. 13a), tongues of dry air were identified on a vertical cross-section of r_v and w in the LES. These tongues were subsiding and some of them even reached the bottom of the CBL. As shown in Fig. 6, they have a conic upside-down shape, reminiscent of the structures identified by Sullivan et al. (1998) under moderate to large Richardson numbers. They penetrate downward from the entrainment zone (EZ), which plays a significant role here as the location where the initial characteristics of the dry tongues are determined. They are a few hundreds metres wide and the lower, thinner, extremity of the dry tongues sometimes splits. Negative anomalies of moisture and vertical velocity characterise these dry tongues. Figures 7b and c show the vertical profiles of respectively r_v and θ, and w and buoyancy in the dry intrusion shown in Fig. 7a; the profiles of r_v and θ averaged over the horizontal domain are also indicated in Fig. 7b. The value of r_v within these tongues is typical of the EZ and increases slightly at lower levels, due likely to mixing (Fig. 7b). The minimum of r_v at 300 m is still around 1.5 g kg^{-1} below the CBL mean value at this same

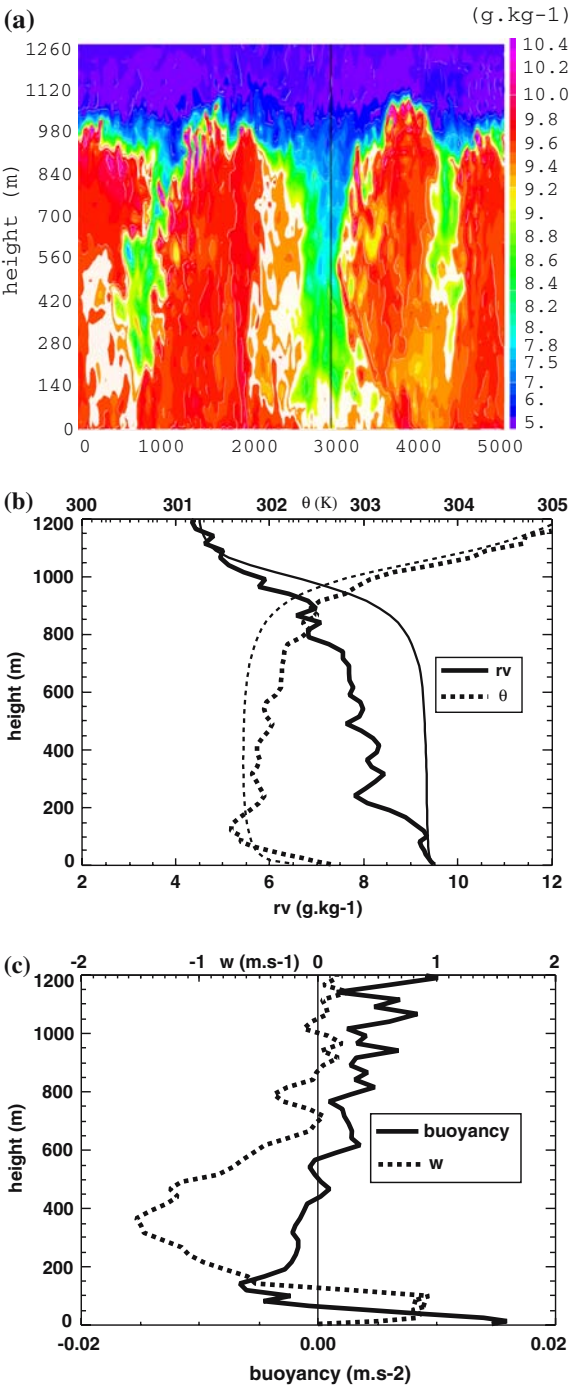

Fig. 7 (**a**) Vertical cross-section of r_v simulated by REF at 1200 LT and vertical profiles of (**b**) r_v and θ and (**c**) buoyancy and w in the dry intrusion (thick line) located by the white line on (**a**). For (**b**) the horizontal-mean values are indicated by thin lines

height. A further decrease of the vertical velocity (which becomes more negative than higher up) is noted around 450 m as the buoyancy becomes negative, suggesting a driving role of buoyancy. As the upper part of the intrusions are positively buoyant (warmer air coming from above the CBL), their descent is thus not initially buoyantly driven at this level but rather dynamically forced. This point is investigated further in Section 4.1.

3.3 Statistical properties

Hereafter, in order to provide a statistical overview of the characteristics of these tongues, a conditional analysis is used and applied to simulation REF. Similar conclusions are obtained for simulation CSTINI. Such an analysis has been widely used in boundary-layer studies (Young 1988; Grossman and Gamage 1995; Berg and Stull 2004). To select the structures, a r'_v threshold value is chosen equal to half of the standard deviation at $0.8z_i$ (Fig. 8a) similarly to Berg and Stull (2004). The analysis is done independently at each vertical level but the threshold is constant (independent of height) ensuring vertical consistency. A minimum size (on each dimension, along x and y, the length of the structure has to be larger than 200 m) has also been prescribed so as to avoid selecting fluctuations due to small-scale turbulence.

Figure 8b presents the total area covered by the selected intrusions at 1200 LT for simulation REF. The structures are more frequent at the top of the CBL where they cover 30% to 35% of the total domain. Their fractional coverage decreases at lower levels because not all of them descend to the bottom of the boundary layer, and also because the dry tongues become thinner at lower levels (Fig. 6). At $0.2z_i$, the structures cover only 5% of the domain. The negative moisture anomaly (r'_v) becomes less pronounced at low levels indicating that mixing with air occurs along the descent, and the vertical velocity becomes more negative down to $0.3z_i$ (Fig. 8c). Similar results are obtained from the same conditional sampling applied to aircraft observations at $0.4z_i$: $r'_v \approx -0.5\,\mathrm{g\,kg^{-1}}, w' \approx -0.3\,\mathrm{m\,s^{-1}}, \theta'_v \approx -0.1\,\mathrm{K}$ and $\theta' \approx 0$). Overall, θ'_v becomes negative at $0.7z_i$ whereas θ' stays mostly positive, underlining the role of water vapour in the buoyancy. Even though quantitative differences are apparent during the simulation, this description is representative of the time period from 1000 to 1400–LT.

To better understand the dynamics of such structures, we have explored how their size depends on selected parameters. The correlation is highest ($r^2 = 0.4$) between structure size and the minimum of r'_v with a relation linking the largest structures to the driest ones throughout the simulation (Fig. 9). This can be understood in terms of 'mixing sensitivity', with larger structures suffering less mixing with the environment, and therefore retaining their dry signature longer.

3.4 Contribution of dry intrusions to CBL properties

The contribution of such dry tongues to the variance of w, θ_v, r_v and the moisture vertical flux is now analysed via conditional sampling. This allows us to quantify the impact of these intrusions on the CBL statistical properties.

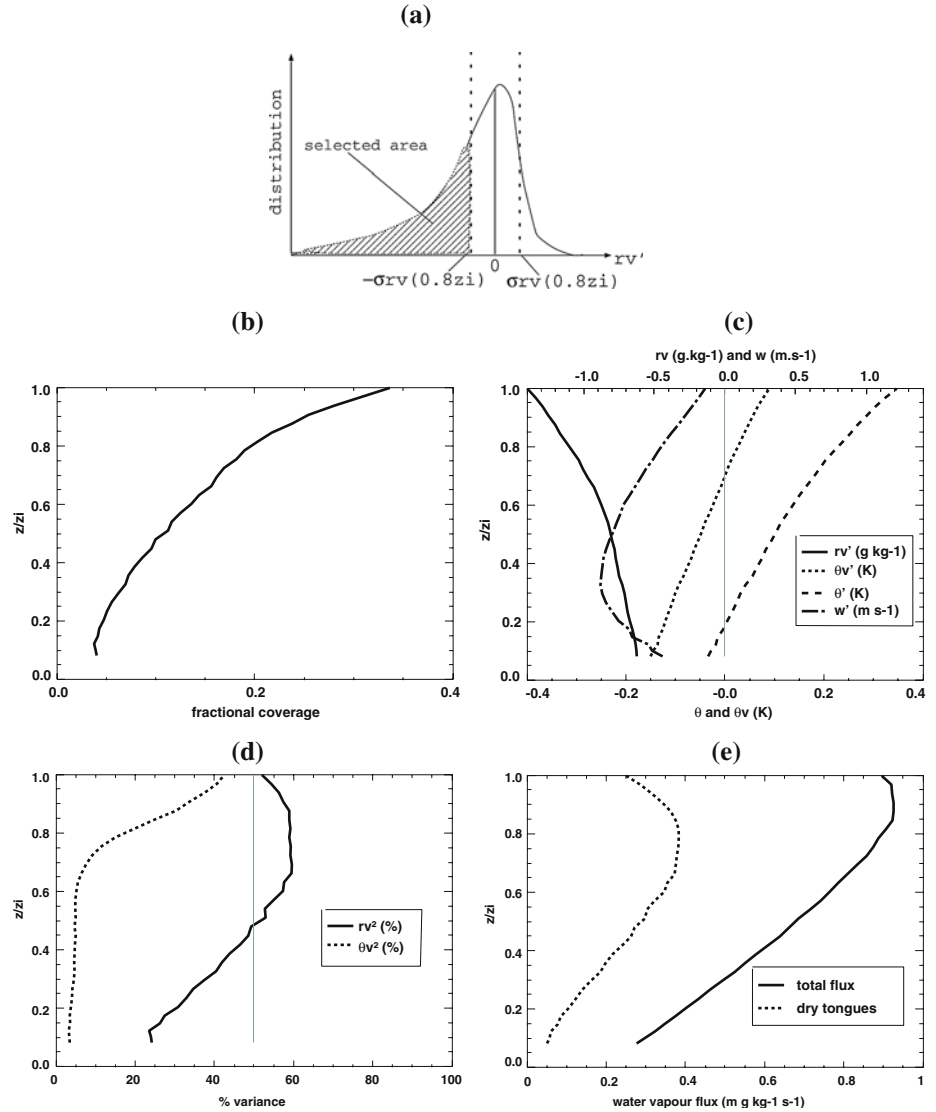

Fig. 8 In the top panel (**a**), the dashed zone corresponds to the points of the r_v distribution selected by the conditional sampling analysis (σ_{rv} is the standard deviation). In the middle panels, the fractional coverage of the air selected is shown on the left (**b**), and, the right panel (**c**) indicates the mean of the different thermodynamical variable fluctuations for the air selected. The bottom left panel (**d**) indicates the variance contribution of the air selected. The bottom right panel (**e**) indicates the total moisture flux (full line) and the contribution of the air selected (dotted line). All these statistics are obtained for the REF simulation at 1200 LT. Similar results are obtained at other times

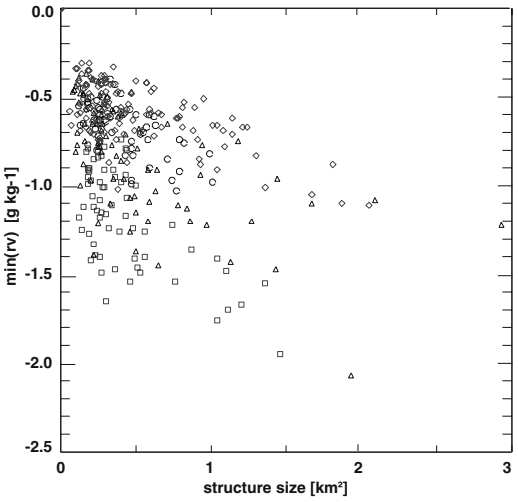

Fig. 9 Minimum of r_v perturbation as a function of the structure size concerned by the dry tongues at $0.3z_i$ and 1100 (circle), 1200 (box), 1300 (triangle) and 1400 (diamond) local times for the REF simulation. The correlation coefficient is $r^2 = 0.4$. The dry tongues are isolated using the conditional sampling analysis

3.4.1 Variance

Very little (5–10%) of the vertical velocity variance is explained by these structures. However, as shown in Fig. 8d, a significant part of the θ_v variance is due to these structures above $0.7z_i$ indicating that the entrainment impacts upon this variance in the upper third of the CBL. The dry tongues explain more than half of the moisture variance from $0.4z_i$ to z_i and still contribute significantly at lower levels. Conditional sampling on aircraft observations at $0.4z_i$ reports consistently around 45% to 50% of the variance explained by the dry tongues. This confirms Druilhet et al. (1983)'s results derived from aircraft in-situ measurement into the CBL from different zones concerning the continental CBL under clear skies. The authors suggested the importance of entrainment for the variance of moisture. The influence of entrainment for the variance of scalars was also previously underlined by Moeng and Wyngaard (1984, 1989) and Moene et al. (2006) in the framework of top-down/bottom-up scalar diffusion.

3.4.2 Moisture flux

Dry tongues contribute less to moisture fluxes than to moisture variance. Nevertheless they contribute to 40% of the moisture fluxes (a similar result is obtained when applied to aircraft observations) despite only covering about 20% of the total area (Fig. 8e). Grossman and Gamage (1995) underlined the importance of structures descending into the CBL from the EZ to account for the total moisture flux at low levels. Our results indicate that the contribution of dry tongues to the moisture flux is significant over the whole depth of the boundary layer.

Figure 10 (left figures) presents the joint distribution of w and r_v. Each graph can be partitioned in four quadrants: NN$\{r'_v < 0, w' < 0\}$ corresponding to the dry tongues, NP$\{r'_v < 0, w' > 0\}$, PN$\{r'_v > 0, w' < 0\}$, and finally PP$\{r'_v > 0, w' > 0\}$, which corresponds to the moist thermals; the mean values are indicated by dashed lines. The numbers correspond to the percentage of total flux explained by each quadrant. If one assumes that the small-scale turbulence is homogeneous and isotropic and therefore impacts equally upon all four quadrants, it can be deduced that, in the middle of the

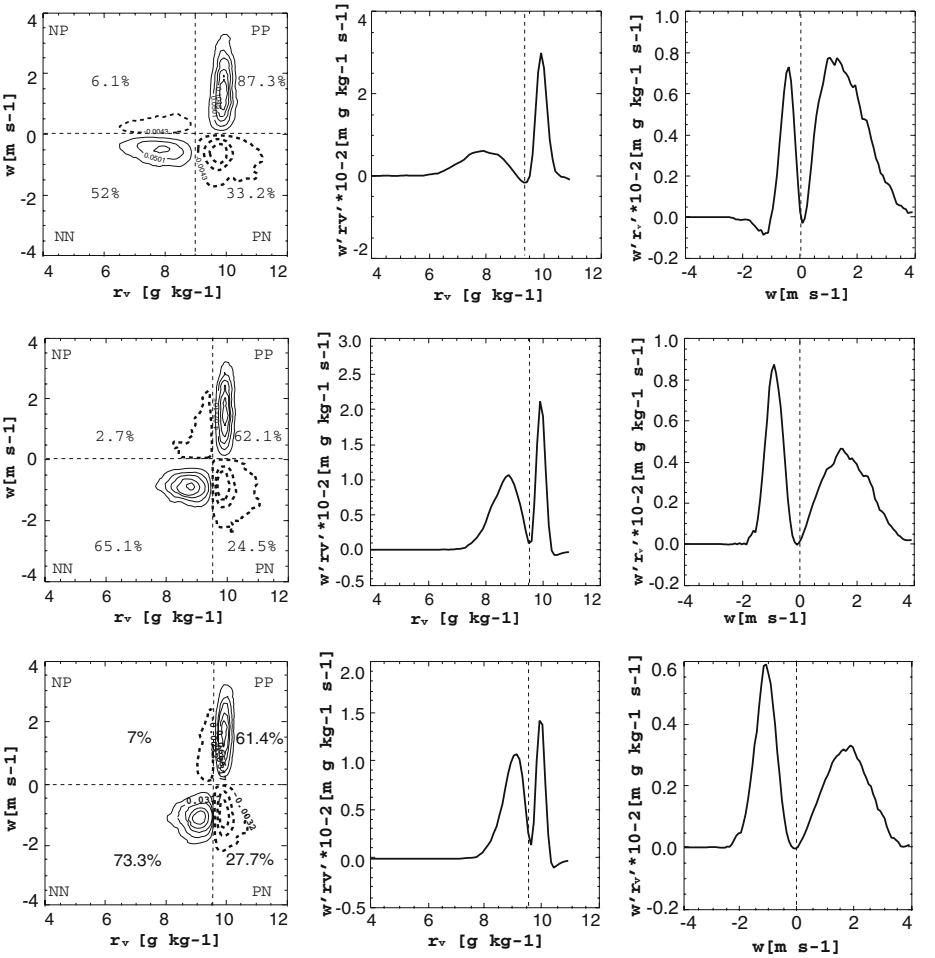

Fig. 10 In the left panels, joint distribution of moisture and vertical velocity at three different heights (from bottom to top, $0.3z_i, 0.5z_i$ and $0.75z_i$) at 1200 LT are shown. Isocontours of moisture fluxes are 0.0089 for $0.3z_i$, 0.0052 for $0.5z_i$ and 0.008 for $0.75z_i$. The numbers correspond to the percentage of the total flux represented by each quadrant. The middle and right panels correspond to the contribution to the moisture flux of respectively water vapour mixing ratios and vertical velocities. The area below the curve corresponds to the total moisture flux (the respective steps for the computation of the distribution is 0.11 g kg^{-1} for water vapour mixing ratio and 0.08 m s^{-1} for vertical velocity)

boundary layer, dry tongues contribute as much as the thermals to the positive moisture flux. In the upper part of the boundary layer, the dry tongues contribution is still significant but inferior to the contribution of the thermals. The percentage explained by the dry tongues is larger at low levels due to the larger vertical velocity. Only at low levels ($0.3z_i$), are all four quadrants significant. At higher levels, the dry air is mainly subsiding (the quadrant NP is almost negligible) while the moist air is largely associated with ascending motions. This figure also shows an asymmetry in PN and NP as in Crum et al. (1987) since the contribution of PN is always larger than that from NP, PN being due to detrainment of moist thermals or entrainment into the

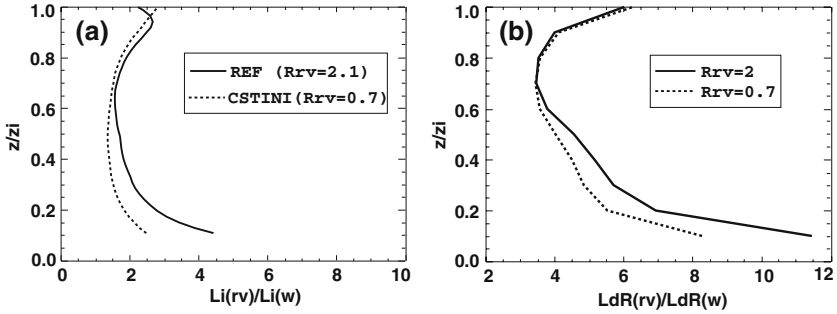

Fig. 11 (**a**) Water vapour mixing ratio integral length scale normalised by the vertical velocity integral length scale at 1300 LT for REF (thick line) and CSTINI (dotted line). (**b**) Water vapour mixing ratio length scale normalised by the vertical velocity length scale calculated according to de Roode et al. (2004) for a water vapour flux ratio, Rr_v, of 2 (thick line) and 0.7 (dotted line). Rr_v is the ratio between the moisture flux at the top of the CBL and the moisture flux at the bottom

dry tongues. Similar asymmetry was noted by Michels and Jochum (1995). The middle (right) panels indicate the contribution of a moisture anomaly (vertical velocity anomaly) to the moisture flux. The negative moisture anomalies, characterised by a large spectrum of values, mainly correspond to NN as NP is almost negligible, at least at $0.5z_i$ and $0.75z_i$. This large spectrum of negative moisture anomalies results from different levels of origin in the EZ for the dry tongues but also for different dilution due to mixing with the environment. Similarly, the positive vertical velocity anomalies mainly correspond to PP. The wide spectrum of positive values underlines different velocities for the thermals, and this illustrates a distinct behaviour between w and r_v: the positively skewed w distribution is mainly explained by the thermal properties whereas the negatively skewed r_v distribution is mainly due to the dry intrusions.

3.4.3 Characteristic length scale

As shown in C05, dry tongues originating from the entrainment layer constrain the characteristic length scale of moisture fluctuations in the CBL. Here the integral length scale is used and defined by $\int_0^{x_o} a(l)dl$ where x_o corresponds to the first zero-crossing of the autocorrelation function $a(l)$, following Lohou et al. (2000); the length scales were computed independently at each vertical level in the simulations. This length scale results from the effect of different processes. Nevertheless, its vertical profile, with higher values at low levels and lower values at upper levels, varies inversely to that of the number of intrusions present in the domain ($10 \times 10\,\mathrm{km}^2$): the number of intrusions varies from 50 at $0.2z_i$ to 140 at $0.8z_i$. Note that for simulation CSTINI, the r_v length scale increases with height up to the middle of the CBL suggesting different processes occurring at lower levels.

The r_v length scale is larger than the θ, θ_v and w length scales, in agreement with Jonker et al. (1999) and de Roode et al. (2004). In de Roode et al. (2004) (dR04 in the following), a length scale was derived according to the spectrum of the variables[3]

[3] The length scale is defined by the critical wavenumber for which the integral of the spectral density between this wavenumber and the Nyquist frequency is equal to 2/3 of the variance.

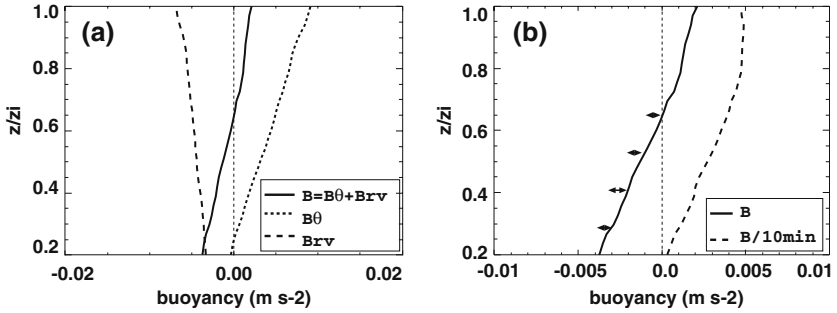

Fig. 12 Vertical profiles of buoyancy in the dry tongues (conditional sampling) around 1200 LT(**a**) with respective contributions from θ (dotted line) and r_v (dashed line) and (**b**) buoyancy and 'buoyancy calculated relatively to the mean profiles 10 min earlier'. The arrows indicate the change in time during this 10 min of the contribution from r_v to the total buoyancy

whereas here the integral length scale is computed. To be able to further compare these distinct length scales, given the different means of calculation, the r_v length scale is normalised by the respective w length scale (Fig. 11). Note that for both calculations the w length scale has a similar profile with a maximum in the middle of the boundary layer and minima close to the ground and at the top of the CBL. This length scale is stationary once normalised by the CBL height. There is a consistency between the ratio of integral length scales and that of the dR04 spectral length scales, agreeing with the relationship linking the length scales and flux ratio shown by dR04. In fact, the differences between simulation CSTINI (flux ratio[4] lower than 1) and simulation REF (flux ratio larger than 1) are qualitatively similar to the differences between two spectral length scales with a flux ratio of 2 and 0.7. A larger length scale at lower levels for simulation REF can be interpreted through the predominance of dry tongues on this characteristic length scale whereas for simulation CSTINI the length scale is more related to moist thermals that are closer to each other.

4 Processes and mechanisms involved in the sign of S

Next, we focus on the processes responsible for the characteristics of these dry tongues and specifically on the sign of S.

4.1 Role of buoyancy

A striking feature of the simulated dry tongues is the acquisition of a negative virtual potential temperature anomaly as tongues subside into the CBL, despite the positive virtual potential temperature anomaly at their initiation (Fig. 8c). To determine the processes involved in the movement of this dry air we focus here on the buoyancy.

The analysis of the vertical velocity budget for the dry tongues (once the hydrostatic contribution has been removed) indicates that the buoyancy term increases the vertical velocity above $0.6–0.7 z_i$ and decreases it below. So the buoyancy term favours descending dry air as the downdraft reaches the neutral buoyancy level. Figure 12a

[4] Here the flux ratio denotes the ratio between the flux at the top of the CBL and the flux at the surface.

shows the mean buoyancy of the dry tongues and the respective contribution of θ and r_v to this buoyancy; it underlines the significant role of r_v in the buoyancy favouring negative buoyancy whereas θ only contributes to positive buoyancy.

The boundary-layer warming in the growing phase plays a role in the acquisition of the negative buoyancy for the dry tongues. At least, this mechanism explains part of the negative buoyancy. In fact, as many dry tongues descend largely isolated from the rest of the CBL, the CBL is warmed by the surface heat flux and dried due to the divergence of the moisture flux. The lifetime of a dry intrusion is around 20 min. As shown in Fig. 12b, the buoyancy of the dry tongues is negative below $0.6z_i$; the buoyancy calculated relative to the mean environment 10 min (half the lifetime) earlier for this dry tongue is positive, underlining the important warming occurring in the environment of the dry tongues. The boundary layer warms and dries during this period of time with the warming having a much stronger impact on the θ_v profile than the drying, resulting in an increase of the mean θ_v. As the dry tongues remain relatively isolated from the rest of the CBL during their subsidence, the role of the warming of the boundary layer in the development of such negative buoyancy is significant. This is also qualitatively coherent with the decrease of the vertical velocity characterizing dry tongues as they penetrate deeper into the CBL (e.g. Fig. 8c, from z_i down to $0.3z_i$).

Both factors, CBL growth and warming, tend to increase the variability of r_v in the CBL but through distinctive mechanisms: the first one increases the quantity of dry air ingested into the CBL which is not instantaneously mixed by turbulent processes, whereas the second one allows for deep penetration. So, CBL warming further enhances the variability generated by the CBL growth. These results are consistent with a more negative S during the experimental BLE cases (faster growing boundary layer) than for the experimental BLH cases (slower growing boundary layer). Moreover, analysis of the aircraft time series of the BLE cases indicates that most of the dry tongues have negative buoyancy.

4.2 Budgets of water vapour mixing ratio variance, third-order moment and skewness

Very few studies focus on the S budget. Yet, the S vertical profile of a boundary layer can not only give insight into boundary-layer characteristics (e.g., EDBL/MBL discussed in Section 1) but also help characterise the transport asymmetry occurring in the boundary layer (Wyngaard 1987). Mahrt (1991), the first to discuss such a budget, used low-level flight measurements to propose a relationship between moisture skewness and moisture flux divergence in the lower part of the boundary layer. This budget was too simplified according to Wulfmeyer (1999) since the contributions from the moisture variance budget were not considered. Wulfmeyer (1999) proposed a more complete budget analysis but lacked the measurements to evaluate all terms in the budget. Here, we take advantage of LES, which provides moisture moments at different levels in the CBL, to infer the S budget. Analysis of the S budget requires the examination of variance and third-order moment budgets, since S results from both moments. The budgets analysed here have been calculated over a 20-min period at 1200 LT; similar behaviour is noted at other times of the simulation. Only levels above $0.1z_i$ are considered, since below this height the budget involves larger contributions from subgrid parameterised terms. Inspection of water vapour moment profiles over this period indicates that these moments can be assumed to be quasi-stationary during this period below $0.8z_i$ (as shown by the low value of the tendency terms in Figs. 13

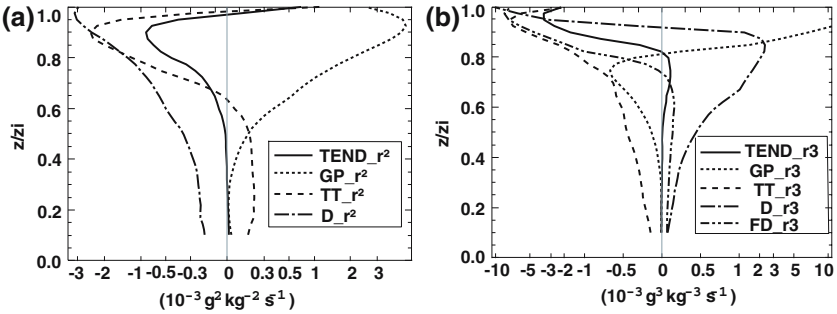

Fig. 13 Boundary-layer budget of water vapour (**a**) variance and (**b**) third-order moments at 1210 LT (corresponding to a 20-min average) for the REF simulation. Note that the x-axis is non-linear in order to show the mixed layer and the entrainment zone budgets

and 15), whereas above the profiles evolve more rapidly in response to the CBL growth. Therefore, in the following, we focus on the budget between $0.1z_i$ and $0.8z_i$ and discuss the processes that maintain this mean state. To our knowledge, it is the first time that such a comprehensive budget of the water vapour mixing ratio moments has been examined in the mixed layer.

Budget equations for the water vapour mixing ratio variance, third-order moment and skewness are given by:

$$\underbrace{\frac{\partial \overline{r_v'^2}}{\partial t}}_{(\mathrm{TEND\_}r^2)} = \underbrace{-2\,\frac{\partial \overline{r_v}}{\partial z}\overline{w'r_v'}}_{(\mathrm{GP\_}r^2)} \underbrace{-\frac{\partial \overline{w'r_v'^2}}{\partial z}}_{(\mathrm{TT\_}r^2)} \underbrace{-D}_{(D)\_r^2} \tag{1}$$

$$\underbrace{\frac{\partial \overline{r_v'^3}}{\partial t}}_{(\mathrm{TEND\_}r^3)} = \underbrace{-3\overline{w'r_v'^2}\frac{\partial \overline{r_v}}{\partial z}}_{(\mathrm{GP\_}r^3)} \underbrace{-\frac{\partial \overline{w'r_v'^3}}{\partial z}}_{(\mathrm{TT\_}r^3)} \underbrace{+3\overline{r_v'^2}\frac{\partial \overline{w'r_v'}}{\partial z}}_{(\mathrm{FD\_}r^3)} \underbrace{-D}_{(D\_r^3)} \tag{2}$$

$$\underbrace{\frac{\partial S}{\partial t}}_{(\mathrm{TEND\_}S)} = \underbrace{\frac{1}{[\overline{r_v'^2}]^{3/2}}\frac{\partial \overline{r_v'^3}}{\partial t}}_{(\mathrm{TEND\_}r^3)} \underbrace{-\frac{3}{2}S\frac{1}{\overline{r_v'^2}}\frac{\partial \overline{r_v'^2}}{\partial t}}_{(\mathrm{TEND\_}r^2)}. \tag{3}$$

The variance tendency (TEND_r^2) results from the gradient production term (GP_r^2), the flux divergence of variance, which corresponds to a turbulent transport term (TT_r^2), and the dissipation (D_r^2) of the variance (Eq. 1). Note that the dissipation is represented in the LES model by subgrid parameterised processes. The third-order moment tendency (TEND_r^3) is due to the gradient production term (GP_r^3), the flux divergence of the third-order moment, which is the turbulent transport term (TT_r^3), the moisture flux divergence (FD_r^3) and the dissipation (D_r^3) of the third-order moment (Eq. 2). The S tendency (TEND_S) combines both former tendencies as shown in Eq. 3. In each of these equations all the terms are explicitly computed except for the dissipation term, which is deduced from the others as a residual from the resolved scales.

4.2.1 Budget in the REF simulation

For the variance budget (Fig. 13a) up to the middle of the boundary layer, the turbulent vertical transport balances the dissipation. Above that level, GP_r^2 becomes significant indicating the increase of turbulent motions occurring within a mean moisture gradient; this gradient is the strongest close to the top of the CBL. D_r^2 tends to destroy $\overline{r_v'^2}$ as reflected in its negative sign and similar vertical structure (Fig. 2c). TT_r^2 becomes negative at $0.7z_i$ (the variance flux divergence decreases with height up to $0.7z_i$ and increases above). In fact, the turbulent transport mainly distributes the variance from the top of the CBL into its interior. Thus, it is mainly a downward transport, moving variance from the region of excess production by the GP_r^2 (upper CBL) to the region of excess destruction by D_r^2 (lower CBL). Indeed, this budget is very similar to that derived for a top-down scalar by Moeng and Wyngaard (1984) underlining the importance of the downward transport. The dry tongues play an important role in this transport as indicated by their significant contribution to the variance flux according to a conditional sampling analysis (not shown). This budget is also in agreement with the results of Lenschow et al. (1980) and Stull (1988), except that, here, TEND_r^2 is not negligible near the top of the boundary layer due to the growth of the boundary layer, which generates significant moisture variance higher up, while decreasing it below (TEND_$r^2 < 0$ below $0.95z_i$).

Before focussing on the $\overline{r_v'^3}$ budget, it is important to recall the vertical profile of $\overline{r_v'^3}$, illustrated in Fig. 2d, with negative values up to 0.9–$0.95z_i$ and positive values at higher levels. The dissipation always tends to destroy the absolute value of the third-order moment as reflected in its systematically opposite sign combined with a similar vertical structure: it is the main loss of $\overline{r_v'^3}$ in the CBL (Fig. 13b). The GP_r^3 becomes significant only above $0.5z_i$, i.e. where the mean vertical gradient of r_v actually increases: it tends to decrease $\overline{r_v'^3}$ below $0.8z_i$ and to increase $\overline{r_v'^3}$ above that level. This complex structure results from entrainment processes across the top of the boundary layer, characterised by strongly varying mean r_v. The FD_r^3 decreases $\overline{r_v'^3}$ from $0.7z_i$ up to z_i due to the decrease of the moisture flux in this layer (Fig. 2b). The turbulent transport term decreases $\overline{r_v'^3}$ over the whole depth of the CBL; in fact, it is this process that produces a downward transport of negative $\overline{r_v'^3}$ from the layer where it is produced by FD_r^3 and GP_r^3, to the layers below where it is destroyed by FD_r^3 and D_r^3. Below $0.5z_i$, it is thus the major, if not the only, source for negative values of $\overline{r_v'^3}$. Conditional sampling of the flux of water vapour moments indicates the significant contribution of the dry tongues (greater than 80% for $\overline{w'r_v'^2}$ and 50% for $\overline{w'r_v'^3}$, from $0.2z_i$ to $0.8z_i$). Finally for this case, the $\overline{r_v'^3}$ budget (Fig. 13b) can be approximated by a first-order balance between the turbulent transport and the dissipation, from $0.1z_i$ to $0.5z_i$.

The budget of S is more complicated as S combines $\overline{r_v'^2}$ and $\overline{r_v'^3}$. Hereafter, we group the different terms as the sum of contributions from the $\overline{r_v'^2}$ and $\overline{r_v'^3}$ budgets. This is done for every term in the same way as is done in Eq. 3 for the tendency term. For example, as shown in Eq. 3, the skewness tendency results from $\overline{r_v'^3}$ and $\overline{r_v'^2}$ tendencies normalised respectively by $\overline{r_v'^2}^{3/2}$ and $\frac{2}{3}\frac{\overline{r_v'^2}}{S}$. Most of the time, these two contributions partially compensate each other (as shown for the GP terms in Fig. 14a, the TT terms in Fig. 14b, in the lower and middle boundary layer, or the TEND terms in Fig. 14c).

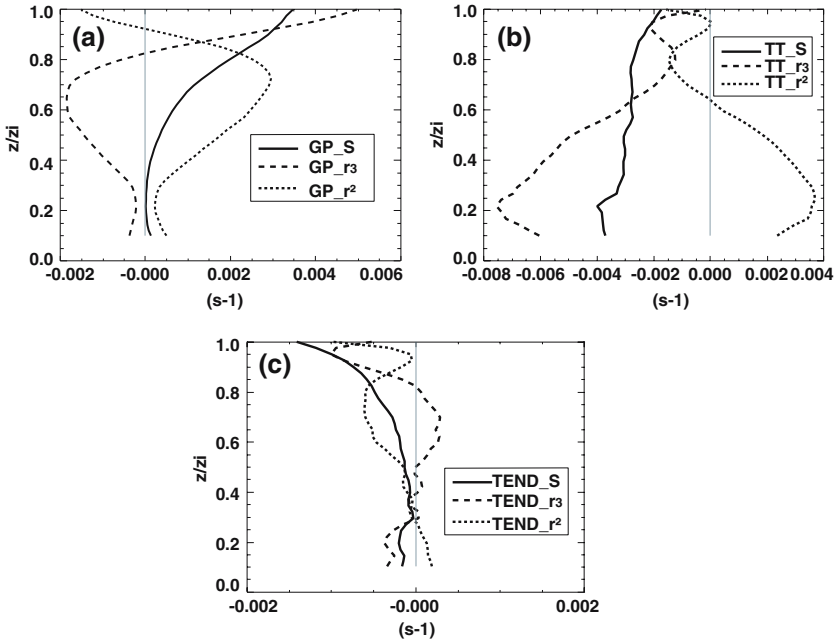

Fig. 14 Contribution of $\overline{r_v'^2}$ and $\overline{r_v'^3}$ terms and the total term in the skewness budget for (**a**) GP terms, (**b**) TT terms and (**c**) TEND terms. These terms are computed at 1210–LT (corresponding to a 20-min average)

They can also both account significantly for the skewness term as shown for these two processes in the upper CBL, underlining the significant contribution of the variance term in the S budget especially from levels $0.4z_i$ to $0.8z_i$. For instance, below $0.8z_i$, the GP_r^3 term produces a decrease of S whereas GP_r^2 tends to increase S. The total contribution of GP_S is an increase of the skewness, indicating that the $\overline{r_v'^2}$ term dominates over the $\overline{r_v'^3}$ term. Therefore, the turbulence created by the mean gradient tends to destroy the negative asymmetry in the CBL. As already discussed by Wulfmeyer (1999), in our case the tendency of S also results from opposite contributions from $\overline{r_v'^2}$ and $\overline{r_v'^3}$. The balance of these two contributions for the different terms varies strongly with height. Above $0.8z_i$, the budget is even more complex but this is beyond the scope of this paper.

Besides these compensation issues, the turbulent transport is again an important factor, bringing negative S from the top of the CBL (Fig. 15a), while all the other processes combine together to reduce the magnitude of this negative S at least below $0.7z_i$. The dissipation tends to destroy any asymmetry as it always has an opposite sign and a similar vertical structure. The only term that has no compensation is the FD_S term as it only appears in the $\overline{r_v'^3}$ budget. This term decreases S in the upper part of the CBL, above $0.75z_i$, and increases it below, in response to the vertical change of the moisture flux (Fig. 2b). This underlines the fact that the flux divergence is not directly responsible for the negative skewness in the lower CBL as it acts to destroy such negative skewness. Indeed, the FD term produces negative skewness in the upper part of CBL, while the downward transport is actually performed by turbulent transport TT_S.

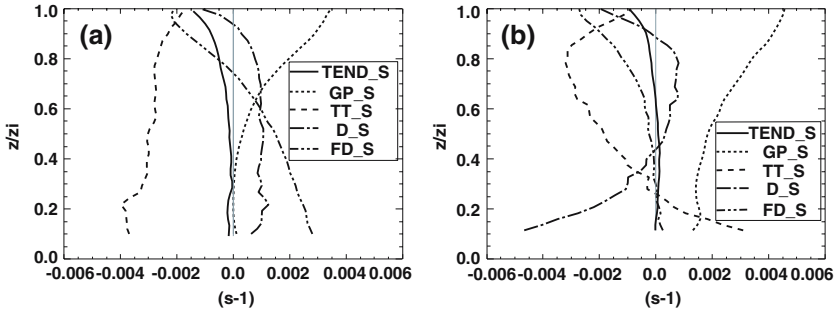

Fig. 15 Boundary-layer budget of water vapour skewness at 1210 LT (corresponding to a 20-min average) for the (**a**) REF and (**b**) CSTINI simulations

Table 2 Summary of the main characteristics of the respective budget of moisture moments for the REF and CSTINI simulations

		TEND			GP			TT			D			FD	
		$\frac{\partial \overline{r_v'^2}}{\partial t}$	$\frac{\partial \overline{r_v'^3}}{\partial t}$	$\frac{\partial S}{\partial t}$	$-2\times$	$-3\overline{w'r}$		$-\frac{\partial \overline{w'r_v'^2}}{\partial z}$	$-\frac{\partial \overline{w'r_v'^3}}{\partial z}$		$\overline{r_v'^2}$	$\overline{r_v'^3}$		$3\overline{r_v'^2}>$	
		$\overline{r_v'^2}$	$\overline{r_v'^3}$	S	$\overline{r_v'^2}$	$\overline{r_v'^3}$	S	$\overline{r_v'^2}$	$\overline{r_v'^3}$	S	$\overline{r_v'^2}$	$\overline{r_v'^3}$	S	$\overline{r_v'^3}/S$	
REF	LBL	>0	**<0**	<0	**>0**	<0	>0	++	**--**	–	–	++	++	+/++	
	MBL	**<0**	>0	<0	+	-	+	++	**--**	–	–	++	++	+/++	
	UBL	-	+	–	++	–	++	–	–	–	–	++	++	–/–	
CSTINI	LBL	>0	**>0**	>0	++	++	++	+	++	++	–	--	–	>0	
	MBL	<0	**>0**	>0	++	<0	++	+	--	–	–	++	+	-	
	UBL	-	>0	<0	++	++	++	-	--	–	–	++	+	-	

TEND stands for tendency term, GP for gradient production term, TT for turbulent transport term, D for dissipation and FD for the flux divergence term. Three distinctive layers are indicated: the lower CBL, LBL, corresponding to levels from 0.1 to $0.3z_i$, the middle of the CBL, MBL, corresponding to levels from 0.3 to $0.7z_i$ and the upper CBL, UBL, corresponding to levels from 0.7 to $0.85z_i$. The intensity is denoted by $>0, +, ++$ from negligible to very significant. The bold signs with grey area designate the process that dominates in the resulting skewness budget

In conclusion, the S budget is complex as $\overline{r_v'^2}$ and $\overline{r_v'^3}$ terms partially compensate each other. The $\overline{r_v'^2}$ terms are important and cannot be neglected, as discussed by Wulfmeyer (1999) even though $\overline{r_v'^3}$ and S have similar signs: it is, for example, the dominant process for the GP term (Table 2). The turbulent transport is significant throughout the whole depth of the CBL, and transports the negative S produced in the upper part of the CBL by the flux divergence term down into the lower part of the CBL. The dry tongues mainly contribute to this turbulent transport. Therefore, it is the complex height-varying balance between TT_S, FD_S and D_S terms that seems to account for the relationship proposed by Mahrt (1991) and shown in Fig. 3.

4.2.2 Budget in the CSTINI simulation

As shown in Fig. 2g, the CSTINI simulation is characterised by a moisture flux convergence and positive S at low levels (Fig. 2j). The negative values at upper levels

emphasise the fact that the Mahrt (1991) relationship is only valid at low levels, and that even in a simulation with moisture flux convergence there is still a strong signature of entrainment in most of the CBL. It is noticeable however that $\overline{r_v'^2}$ and $\overline{r_v'^3}$ are one to two orders of magnitude lower in the CSTINI simulation (Figs. 2h, i) than in the REF simulation (Figs. 2c, d), even though they eventually lead in CSTINI to magnitudes of S comparable to those obtained for REF. Here we analyse the differences between the different r_v moment budgets derived from the CSTINI and REF simulations, in order to precisely determine how the processes combine to produce these distinct S.

The differences between the REF and CSTINI $\overline{r_v'^2}$ budgets are consistent with the surface r_v fluxes playing a relatively more important role as a source of r_v variability in the CBL in CSTINI than in REF, in broad agreement with Moeng and Wyngaard (1984). As shown in Table 2, there is a balance between GP_r^2, D_r^2 and TT_r^2 with a dominance of the first two terms. However, the upper part of the CBL is still significantly affected by processes occurring in the entrainment zone.

Regarding the $\overline{r_v'^3}$ budget in the upper part of the CBL, the balance between the different terms is close to that obtained for REF. Nevertheless, as for the $\overline{r_v'^2}$ budget, the impact on the surface is significant below $z_i/3$ with a positive contribution of GP_r^3 and TT_r^3. Note also that the contribution of the dry tongues for the flux of the water vapour moments is much less in CSTINI than in REF as surface processes play a major role in the CSTINI simulation.

The resulting S budget therefore differs significantly from the REF budget in the lower part of the CBL (Fig. 15b). As D_S still tends to destroy any asymmetry, its vertical structure is modified accordingly (different structures of S). The TT_S term reflects a preponderance of downward transport of negative S from the CBL top down to $0.3z_i$ and of upward transport from the CBL bottom up to the same level. Then, the FD_S becomes significant only above $0.6z_i$, in response to the flux convergence at the top of the CBL creating negative S. In this budget, GP_S has a relatively greater role in the lower and middle regions of the CBL than in REF mainly due to the third-order term, as shown on Table 2. Note that in this simulation, as S changes sign with altitude, the processes involved in the S budget show large and complex fluctuations with height. This stresses the limitations expected from an analysis that is based on too few vertical levels.

In summary, even though these two cases cannot be considered as ideal prototypes as used by Mahrt (1991), they provide useful information about the behaviour of a typical CBL. The relationship between the flux divergence and the S sign seems only valid in the lower part of the boundary layer where it was assessed by Mahrt (1991), even though there is no direct relation as assessed by the budget analysis. In the upper part of the CBL, a strong signature of entrainment is noted in both simulations. The S budget also underscores the main role of the turbulent transport, which distributes the S produced at the top (for REF) or the top and bottom (for CSTINI) of the boundary layer into the whole CBL. The GP term is nearly absent in the lower CBL for REF whereas it is significant for CSTINI. For the GP and TT terms, the differences are mainly due to the third-order moment, even though there is also a significant enhancement of the GP term by the variance in CSTINI.

5 Conclusions

Evidence of dry tongues, their statistical properties, their importance and the mechanisms involved in their growth have been presented in this study using IHOP_2002 observations and LES simulations. These structures are common, and have a large impact on the statistics of water vapour variability even down to levels close to the surface. Particularly, they are responsible for negative moisture skewness in the CBL. They correspond to air from the entrainment zone sinking down into the boundary layer while gradually mixing with the environment, and acquiring negative buoyancy near the middle of the boundary layer. This evolution is also partly due to the strong warming of the CBL in the late morning as the dry tongues remain relatively isolated from the rest of the CBL, which is warmed and dried during its growth. Both the warming and the growth of the CBL increase the r_v variability but through distinct mechanisms. This explains why more negative values of S are observed during the growing phase of the boundary layer.

These dry tongues play a significant role in the CBL moisture-related statistical properties despite their relatively small fractional area. They contribute predominantly to the moisture variance, explaining more than 50% above $0.4z_i$. They also contribute to the moisture flux even though to a lesser extent.

A comprehensive analysis of the moisture variance, the third-order moment and skewness budgets in the whole CBL was conducted for the first time using LES. The S budget is complex: it can significantly vary with height and involves $\overline{r_v'^2}$ terms and $\overline{r_v'^3}$ terms that partially compensate one another. It has been emphasized that to obtain a comprehensive budget of S, the $\overline{r_v'^2}$ terms have to be taken into account even though $\overline{r_v'^3}$ and S have the same sign. This analysis also shows the importance of the turbulent transport term in the entire budget. The sign of S appears to result from the opposition between upward (bringing positive S from the surface) and downward transport (bringing negative S from the top of the CBL). In agreement with Mahrt (1991), we found that a positive (negative) S in the lower CBL was associated with a negative (positive) divergence of the turbulent CBL moisture flux. The complexity of the S budget is, however, indicative of the difficulties one may encounter in determining more quantitative relationships between these two quantities.

In this study, the role of wind shear has not been studied. It probably also plays a role, as shear can destabilise the dry tongues and decrease their lifetime and hence their chance of reaching low levels.

Here, the dry tongues have been emphasized during spring over the southern Great Plains of the USA. Nevertheless, dry tongues originating from the CBL top and descending deeply into its interior are also apparent in a numerical simulation of a Sahelian convective boundary layer under semi-arid conditions (Lothon et al. 2005) and evidence of such features are indicated from aircraft measurements over the same area. It is likely that such CBL characteristics are common over large areas, with a seasonal dependency. An open question regarding these CBL features concerns what they may reveal of CBL behaviour. Specifically, is there a general relationship between moisture skewness and moisture flux divergence as partly assessed by the present study?

Moreover, as these dry tongues contribute significantly to the moisture variance and flux, their possible representation in CBL parameterizations should be investigated in order to improve the moisture distribution predicted by mesoscale models.

Acknowledgements The authors are grateful to T. Weckwerth and two anonymous reviewers for their helpful comments and suggestions. They also thank K. Craig for the retrieval of boundary-layer depths from lidar data, S. Williams for the help about soundings, B. Geerts for KA data, S de Roode for the length scale data and P. Jabouille and more broadly the Meso-NH team. Eventually, the lead author also thanks P. Austin for a reading of the previous form of the manuscript. This research has been supported by the GAME (CNRS-Météo-France).

References

Berg L, Stull RB (2004) Parameterization of joint frequency distributions of potential temperature and water vapour mixing ratio in the daytime convective boundary layer. J Atmos Sci 61:813–828

Coulman CE (1978) Boundary-layer evolution and nocturnal dispersal – part II. Boundary-Layer Meteorol 14:493–513

Couvreux F, Guichard F, Redelsperger J-L, Kiemle C, Masson V, Lafore J-P, Flamant C (2005) Water vapour variability within a convective boundary layer assessed by Large Eddy Simulations and IHOP_2002 observations. Quart J Roy Meteorol Soc 131:2665–2693

Crum TD, Stull RB (1987) Field measurements of the amount of surface layer air versus height in the entrainment zone. J Atmos Sci 44:2743–2753

Crum TD, Stull RB, Eloranta EW (1987) Coincident lidar and aircraft observations of entrainment into thermals and mixed layers. J Climate and Appl Meteorol 26:774–788

Cuxart J, Bougeault P, Redelsperger JL (2000) A turbulence scheme allowing for mesoscale and large eddy simulations. Quart J Roy Meteorol Soc 126:1–30

Davis KJ, Gamage N, Hagelberg C, Lenschow DH, Kiemle C, Sullivan PP (2000) An objective method for determining atmospheric structure from airborne lidar observations. J Atmos Oceanic Tech 17:1455–1468

de Roode SR, Duynkerke PG, Jonker HJJ (2004) Large-eddy simulation: how large is large enough? J Atmos Sci 61:403–421

Druilhet A, Frangi J, Guedalia D, Fontan J (1983) Experimental studies of the turbulence structure parameters of the convective boundary layer. J Climate and Appl Meteorol 22:593–608

Grossman RL, Gamage N (1995) Moisture flux and mixing processes in the daytime continental convective boundary layer. J Geophys Res 100(D12), 25,665–25,674

Jonker HJJ, Duynkerke PG, Cuijpers JWM (1999) Mesoscale fluctuations in scalars generated by boundary layer convection. J Atmos Sci 56:801–808

Lafore J-P et al. (1998) The Meso-NH atmospheric simulation system. part I: adiabatic formulation and control simulations. Ann Geophys 16:90–109

Lenschow DH, Wyngaard JC, Pennell WT (1980) Mean field and second moment budgets in a baroclinic, convective boundary layer. J Atmos Sci 37:1313–1326

Lenschow DH, Wulfmeyer V, Senff C (2000) Measuring second-through fourth-order moments in noisy data. J Atmos Oc Tech 17:1330–1347

Lohou F, Druilhet A, Campistron B, Redelsperger J-L, Said F (2000) Numerical study of the impact of coherent structures on vertical transfers in the atmospheric boundary layer. Boundary-Layer Meteorol 97:361–383.

Lothon, M, Couvreux F, Donier S, Guichard F, Lacarrère P, Saïd F (2005) Organized structures in the Sahelian boundary layer during the transition period between the wet and dry seasons. Proc First Int Conf on African Monsoon Multiscale Analysis, Dakar, December, pp 3–8

Mahrt L (1991) Boundary layer moisture regimes. Quart J Roy Meteorol Soc 117:151–176

Michels BI, Jochum AM (1995) Heat and moisture flux profiles in a region with inhomogeneous surface evaporation. J Hydrol 166:383–407

Moene AF, Michels BI, Holtslag AAM (2006) Scaling variances of scalars in a convective boundary layer under different entrainment regimes. Boundary-Layer Meteorol DOI 10.1007/s10546–006–9053–9

Moeng C-H, Wyngaard JC (1984) Statistics of conservative scalars in the convective boundary layer. J Atmos Sci 41:3161–3169

Moeng C-H, Wyngaard JC (1989) Evaluation of turbulent transport and dissipation closures in second-order modeling. J Atmos Sci 46:2311–2330

Stull RB (1988) An introduction to boundary layer meteorology. Kluwer Academic Publishers, Dordrecht, 666 pp

Sullivan PP, Moeng C-H, Stevens B, Lenschow DH, Mayor SD (1998) Structure of the entrainment zone capping the convective atmospheric boundary layer. J Atmos Sci 55:3042–3064

Tuzet A, Guillemet B, Isaka H (1983) Interfacial scales of temperature and humidity fluctuations in the convective mixed layer. J Rech Atmos 17:185–197

Vila-Guérau de Arellano J, Gioli B, Miglietta F, Jonker HJJ, Baltink HK, Hutjes RWA, Holtslag AAM (2004) Entrainment process of carbon dioxide in the atmospheric boundary layer. J Geophys Res 109, D18110, doi:10.1029/2004.ID004725

Weckwerth TM, Wilson JW, Wakimoto RM (1996) Thermodynamic variability within the convective boundary layer due to horizontal convective rolls. Mon Wea Rev 124:769–784

Weckwerth TM et al. (2004) An overview of the International H20 Project (IHOP_2002) and some preliminary highlights. Bull Amer Meteorol Soc 85:253–277

Wulfmeyer V (1999) Investigation of humidity skewness and variance profiles in the convective boundary layer and comparison of the latter with large eddy simulation results. J Atmos Sci 56:1055–1076

Wyngaard JC (1987) A physical mechanism for the asymmetry in top-down and bottom-up diffusion. J Atmos Sci 44:1083–1087

Young GS (1988) Turbulence Structure of the Convective Boundary Layer. Part II. Phonenix 78–Aircraft Observations of Thermals and Their Environment. J Atmos Sci 45:727–735

Young GS, Cameron BK, Hebble EE (2000) Observations of the entrainment zone in a rapidly entraining boundary layer. J Atmos Sci 57:3145–3160